Contrib Mineral Petrol (2004) 147: 189–200
DOI 10.1007/s00410-003-0551-1

ORIGINAL PAPER

Geoffrey David Bromiley · Hans Keppler

An experimental investigation of hydroxyl solubility in jadeite and Na-rich clinopyroxenes

Received: 8 August 2003 / Accepted: 1 December 2003 / Published online: 7 February 2004

Abstract The solubility and incorporation mechanisms of water in synthetic, water-saturated jadeite and Na-rich clinopyroxenes have been experimentally investigated. Infrared spectra for water-saturated jadeite synthesised from 2.0 to 10 GPa show two prominent sharp peaks at 3,373 and 3,613 cm^{-1} together with several weaker features in the OH-stretching region, indicating that there are at least 5 distinct modes of hydrogen incorporation in the structure. Water solubility in pure jadeite reaches a maximum of about 450 ppm by weight at 2 GPa and slowly decreases with increasing pressure to about 100 ppm at 10 GPa. Solubility can be described by the function $c_{OH} = A\, f_{H2O}^{0.5} \exp(-P\Delta V_{Solid}/R\ T)$, where c_{OH} is water solubility in ppm H_2O by weight, A is 7.144 ppm/$bar^{0.5}$, f_{H2O} is water fugacity, and $\Delta V_{Solid} = 8.019$ cm^3/mol is the volume change of the clinopyroxene upon incorporation of OH. Jadeite provides a good model for understanding hydrogen incorporation mechanisms in more complex omphacite compositions. Assignment of absorption bands in IR spectra verifies the importance of cation vacancies on the M2 site in providing mechanisms for hydrogen incorporation. However, results also suggest that substitution of lower valency cations onto the M1 site may also be important. Solid solution of jadeite with diopside and in particular, with Ca-Eskola component leads to a drastic increase of water solubility, and the bulk composition has a more important effect on the capacity of omphacite to store water than pressure and temperature. Omphacite is expected to be the major carrier of water in a subducted eclogite after the breakdown of hydrous minerals.

Editorial responsibility: W. Schreyer

G. D. Bromiley (✉)
Bayerisches Geoinstitut, Universität Bayreuth,
95440 Bayreuth, Germany
E-mail: geoffrey.bromiley@uni-bayreuth.de
Tel.: +49-921-553744
Fax: +49-921-553769

H. Keppler
Institut für Geowissenschaften,
Universitaet Tübingen, 72074 Tübingen, Germany

Introduction

Subduction of the oceanic lithosphere provides a mechanism for recycling significant volumes of water back into the earth's deep interior. Most models for water transport in subducting slabs assume that water is incorporated in hydrous phases, and that a significant proportion of this water can be carried beyond the depths of arc-magmatism. However, experimental investigations have suggested that most hydrous phases will break down at pressures above 3.0 GPa between 650 and 750 °C and between 700 and 800 °C in typical ultramafic and basaltic compositions, respectively (Bromiley and Pawley 2002; Schmidt and Poli 1998). Retention of hydrous phases may only occur in the coolest parts of the subducting slab, if at all. In contrast, investigations of natural samples from mantle xenoliths have demonstrated that a number of nominally anhydrous minerals (NAMs) contain small, yet significant, amounts of water in the form of structurally-bound hydrogen, under upper-mantle conditions (Bell and Rossman 1992; Ingrin and Skogby 2000). Of the numerous minerals investigated, clinopyroxene is the major upper-mantle mineral demonstrated to contain the highest concentrations of hydroxyl. Of particular importance in terms of water recycling during subduction could be the clinopyroxene omphacite. Omphacite is a diagnostic mineral of ultra-high-pressure rocks, and its association with coesite and garnet is characteristic of eclogites from high-pressure terrains. Evidence from such high-pressure terrains and from experimental investigations have demonstrated that omphacite is stable over the entire pressure–temperature range expected for subducting slabs in the upper mantle (Green et al. 2000; Schmidt 1993).

In simplistic terms, *C*2/*c* omphacites can be considered solid solutions between jadeite ($NaAlSi_2O_6$) and

diopside ($CaMgSi_2O_6$) end members. However, natural omphacites usually have considerably more complex compositions, which can be modelled in terms of solid solutions involving a number of additional end-member pyroxenes: for example, $NaFe^{3+}Si_2O_6$ (aegirine), $CaAl_2SiO_6$ (Ca-Tschermak component), $CaFe^{2+}Si_2O_6$ (hedenbergite), $Ca_{0.5}\square_{0.5}AlSi_2O_6$ (Ca-Eskola component). Cameron and Papike (1981) and Rossi et al. (1983) give detailed reviews of the crystal chemistry of omphacitic pyroxenes. Jadeite- and diopside-rich pyroxenes have the $C2/c$ space group, with an octahedral M1 site and a (6 + 2) coordinated M2 site. Intermediate compositions show ordering of Mg and Al and of Ca and Na, which implies a lowering of the symmetry to $P2/n$ at temperatures below 750 °C. Above this temperature, all omphacites are $C2/c$. Under upper mantle conditions, all omphacites are also expected to have the $C2/c$ space group.

Incorporation of hydroxyl in natural omphacites from mantle xenoliths was investigated by Smyth et al. (1991), following a previous report of high water contents in a natural omphacite by Skogby et al. (1990). Smyth et al. (1991) used polarized Fourier-transform infrared (FTIR) spectroscopy to investigate hydroxyl incorporation in a number of omphacites with varying compositions. They found that spectra varied largely as a function of composition along the jadeite–diopside tie-line, with the highest water contents recorded for jadeite-rich omphacites with nominal Ca-Eskola contents (i.e. vacancies on the M2 site). In fact, Smyth et al. (1991) noted a positive correlation of absorbance (due to structurally incorporated hydrogen) with vacancy content for the samples studied. Experimental investigations (Gasparik 1986; Malinovskaya et al. 1991) have demonstrated that high vacancy contents in pyroxenes are likely to be stabilised under upper-mantle conditions. There is also considerable evidence from high-pressure eclogitic terrains that high-vacancy contents may be stable in pyroxenes at high-pressure. Pyroxenes from such terrains commonly exhibit exsolved lamellae of phases such as garnet, kyanite, hornblende, various pyroxenes, K-feldspar, mica and silica (e.g. Schmädicke and Müller 2000; Zhang and Liou 1999; Zhang et al. 1997). Recalculation from host and exsolved phase compositions frequently suggests that the precursor phase was a $C2/c$ pyroxene with considerable cation deficiencies and often with high-water contents (Terry et al. 2003). Using such a recalculated pyroxene composition with 18% vacant M2 sites, and their correlation of number of vacancies with hydroxyl content, Smyth et al. (1991) calculated a theoretical high-pressure pyroxene precursor with up to 4,000 ppm OH. There is, therefore, considerable evidence to suggest that omphacite could be one of the most important repositories for water in subducting slabs beyond the stability of hydrous phases.

Despite the possible importance of omphacite there has been, to date, no comprehensive experimental investigation of hydroxyl incorporation. Considerable work has been performed on hydroxyl incorporation in both natural and synthetic diopside (e.g. Rauch 2000; Skogby 1994; Skogby et al. 1990; Smyth et al. 1991), although only a few spectra have been published for synthetic jadeite (Rauch 2000). This is probably due to the inherent problems of synthesizing phases at high-pressure which are of a suitable size and quality for study of hydroxyl incorporation, especially using single-crystal FTIR spectroscopy, a technique that requires large (over 50 μm) crack- and inclusion-free samples. In addition, the composition of omphacite varies considerably as a function of pressure, most notably in the Ca-Eskola component, but also probably in the Ca-Tschermak component (Malinovskaya et al. 1991). Such variations as a function of pressure and temperature are still poorly constrained, but probably have a dominating influence on the mode and quantity of hydroxyl incorporation.

The aim of the present study is to investigate hydroxyl incorporation in synthetic jadeite as a function of increasing pressure up to 10 GPa. In addition, the effects of additional components (diopside, Ca-Eskola) on the incorporation of hydroxyl will be investigated.

Experimental methods

Sample synthesis

For synthesis of water-saturated jadeite, two methods were used to produce crystals of a suitable size and quality for investigation of hydroxyl incorporation using FTIR spectroscopy. Method 1 was used to synthesize samples up to 4 GPa using an end-loaded piston-cylinder apparatus. For these experiments, a starting mix of sodium tetrasilicate glass ($Na_2Si_4O_9$) and $Al(OH_3)$ (Merck, high-purity containing less than 100 ppm iron) was used. Sodium tetrasilicate glass was made from a mixture of Na_2CO_3 (99.995%) and SiO_2 (99.999%) that was decarbonated by slowly heating the mix to 1,100 °C. A homogeneous glass was produced by heating the ground mixture in a platinum crucible at 1,100 °C for 2 h, and then plunging the crucible in water. The resulting glass was finely ground. Optical examination revealed that complete vitification had occurred. The composition of the glass was checked using ICP-AES to ensure that no sodium-loss had occurred. The finely-ground sodium tetrasilicate glass and $Al(OH)_3$ were ground under ethanol for 2 h to produce a completely homogeneous starting mix. The starting mix was loaded into 10-mm long, 5-mm o.d., 4.6-mm i.d. $Pt_{95\%}Rh_{5\%}$ capsules with approximately 5 wt % excess silica and 20 wt % distilled water. Capsules were placed in pyrophyllite sleeves and loaded into 0.5 inch talc-pyrex sample assemblies. These sample assemblies contained an internal, tapered, graphite resistance furnace to ensure minimal temperature gradients along the length of the capsule. Temperature gradients are estimated to be less than 25 °C for the experimental conditions used (Bromiley, unpubl. data). Pressure was calibrated against the quartz–coesite and kyanite–sillimanite transitions, as well as the melting point of diopside, and pressures are accurate to within less than ±5% of the stated value. Temperature was measured with a $Pt\text{-}Pt_{10\%}Rh$ thermocouple. No correction for the effects of pressure on thermocouple EMF was applied. Experiments were pressurized to within 90% of the desired run pressure and then heated at 100 °C/min to 1,000 °C, before being fully pressurized. This temperature is considerably higher than the melting point of the starting mix (which is sodium and water-rich). Run temperature was maintained at 1,000 °C for approximately 24 h to ensure that a completely homogeneous melt

formed, and then slowly ramped down to 600 °C at a rate of 10 °C min. The run temperature was then maintained at 600 °C for 1 week or longer.

Using method 1, jadeite crystals of a suitable size and quality for infrared measurements were synthesized. Experiments performed below 2 GPa produced albite and quartz. Jadeite breaks down at pressures below 1.8 GPa according to the reaction albite = jadeite + quartz (Holland 1990). For the water and silica-rich bulk composition used, the position of this reaction appears to be at slightly higher pressure than determined by Holland (1990). For experiments at 2.0 GPa and above, a marked decrease in crystal size for jadeite with increasing pressure was noted. Above 4 GPa, crystals were below a few tens of microns in size, and were no longer adequate for FTIR spectroscopy. Therefore, an alternative method, method 2, was used. For experiments up to 10 GPa, 2 mm o.d., 3.5-mm-long Pt capsules were used for use in a Walker-cell type multi-anvil apparatus (Walker 1991; Walker et al. 1990). Capsules were half-filled with a layer of SiO_2 and half with a layer of nepheline glass ($NaAlSiO_4$) together with 10 wt % water. Nepheline glass was made from a mixture of SiO_2, Na_2CO_3 and $Al(OH)_3$ using the same method outlined above for sodium tetrasilicate glass (except with heating at 1,600 °C). Capsules were loaded into MgO ceramic octahedra with internal, stepped, graphite resistance heaters. The temperature gradient along the length of the capsule is probably less than 50 °C. 18 M Toshiba-grade tungsten-carbide anvils were used. Temperatures were measured using a $W_{3\%}Rh$–$W_{27\%}Rh$ thermocouple. Samples were fully pressurized, and then slowly heated at 100 °C/min to 700 °C. Run temperature was maintained for 53–103 h. Pressure was calibrated against the wollastonite-perovskite and coesite-stishovite phase transitions, and is accurate to within ±5%. Both piston-cylinder and multi-anvil apparatus experiments were quenched isobarically by shutting off the power to the heating circuit whilst maintaining run pressure.

In addition to synthesis of pure jadeite, two more complex bulk compositions were used to study the effects of additional components on hydrogen incorporation. Starting mixes were made with bulk compositions of $Jd_{0.76}Di_{0.24}$ and $Jd_{0.9}Ca\text{-}Es_{0.1}$ (where Jd = jadeite, Di = diopside, and Ca-Es = Ca-Eskola), using sodium metasilicate (Na_2SiO_3; prepared using the method described for sodium tetrasilicate glass) and sodium tetrasilicate glass, respectively, and $Al(OH)_3$, $Mg(OH)_3$ (Fluka, 99%+), $Ca(OH)_2$ (Aldrich, 99%+) and SiO_2 (99.999%). Starting mixtures were ground under ethanol for 2 h and compositions checked using ICP-AES. These starting materials were run in the piston cylinder apparatus using similar procedures as outlined above under method 1.

Phase identification and chemical analysis

After the experiments, capsules were recovered and cut lengthwise. Figure 1 shows two sectioned capsules from experiments using methods 1 and 2 respectively. For experiments preformed using method 1, elongated to needle-shaped jadeite crystals were produced. Crystals were elongated along the c-axis, and ranged up to 1 mm in length. However, crystal size in all other dimensions was considerably smaller, sometime only a few tens of microns. For experiments with more complex bulk compositions, crystal size was notably smaller. Crystals appeared to have nucleated on the walls of the capsule and grown inwards into a central, fluid-rich cavity. In addition to jadeite and omphacite, quartz or coesite crystals were noted in all samples, along with the presence of very fine-grain, silica-rich quench material. Individual pyroxene crystals, or small clusters of crystals, were plucked from the halved capsules and prepared for infrared measurements. Other crystals were taken for phase identification using a Dilor labram Raman spectrometer equipped with a 20 mW HeNe laser and a microscope, and then placed in resin and prepared as grain mounts for microprobe analysis. A Cameca SX50 electron microscope operating at 15 kV and 15 nA was used for sample analysis using the following standards: albite (Na), spinel (Al), SiO_2 (Si), Pt metal, Rh metal, wollastonite (Ca) and enstatite (Mg), with a count time of 20 s for all elements.

For experiments performed using method 2, one halve of the sample was polished down to a doubly polished 100-μm-thick slab for FTIR and micro-Raman measurements. The other halve of the capsule was placed in resin and polished for microprobe analysis.

Infrared Spectroscopy

Near-infrared spectroscopy was used to investigate hydroxyl incorporation in the synthetic samples. Infrared spectra were taken using a Bruker IFS 120 HR high-resolution FTIR spectrometer coupled with a Bruker IR microscope containing all-reflecting Cassegranian optics. The spectrometer contains a permanently aligned Michelson-type interferometer with a 30° angle of incidence on the beam-splitter. Measurements were taken using a tungsten light source, a Si-coated CaF_2 beamsplitter and a narrow-band MCT detector. Several hundred scans were acquired for each spectrum. Polarized spectra were recorded using a wire-strip polarizer on a KRS-5 substrate. The optics of the microscope were purged with H_2O- and CO_2-free purified air during measurements, and the optics of the spectrometer were kept under vacuum to prevent absorption bands caused by water vapour.

FTIR absorption spectra were obtained from optically clear areas of crystals. Rauch and Keppler (2002) demonstrated the importance of obtaining spectra from crack- and inclusion-free areas of crystals for accurate determination of water contents. Variable rectangular apertures in the rear focal plane of the 15x Cassegranian objective were used. All samples were placed on CaF_2 plates and immersed in poly-trichlorofluoroethylene oil to prevent the occurrence of interference fringes.

Because of the lack of mineral specific calibrations for jadeite or other compositions studied, concentrations of hydroxyl groups were determined using the frequency-dependent calibration of extinction coefficients by Paterson (1982). In this method, the entire infrared absorption spectrum is divided by a frequency dependent extinction coefficient, and the water content determined by numerical integration of the result over the entire frequency range where absorption due to OH bonds is observed. This calibration is derived from measurements of hydroxyl in quartz and silicate glasses, which raises some doubt as to its general applicability. However, a more recent calibration by Libowitzky and Rossman (1997), based on a number of different hydrous minerals with varying water contents, is in close agreement with the calibration of Paterson (1982).

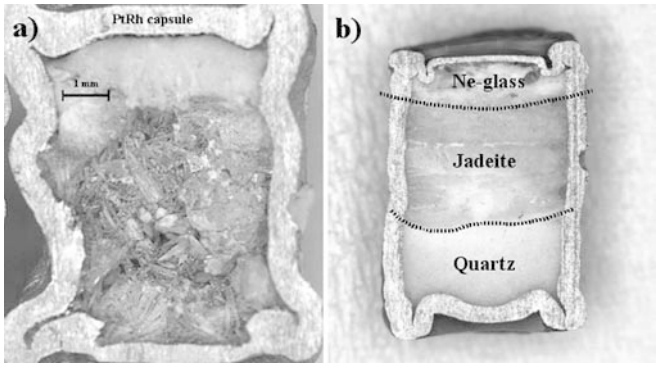

Fig. 1 Recovered capsules from jadeite-synthesis experiments, cut lengthwise. **a** experiment using method 1 showing growth of elongate to needle-shaped jadeite crystals. **b** experiment using method 2, showing growth of jadeite at the interface between layers of quartz and nepheline glass. Both experiments were performed at 2 GPa, using 10-mm-long $Pt_{95\%}Rh_{5\%}$ capsules

Libowitzky and Rossman (1997) noted that determination of water contents based on unpolarized radiation may give misleading results because of anisotropy of absorption bands. In order to determine water contents more accurately, spectra should be taken using polarized radiation parallel to the three main axes of the indicatrix. However, only in lower pressure samples were crystal sizes sufficient for orientation. Therefore, water contents were determined using unpolarized radiation. In order to minimize error in calculated values due to absorption band anisotropy, spectra were obtained from between 20 and 40 crystals for each sample, and from crystals in as many orientations as possible, and the results averaged.

In addition to using unpolarized radiation, additional spectra were taken using polarized radiation. Elongated to needle-shaped crystals (elongated along the c-axis), were selected and aligned optically, and prepared as 100-μm-thick double-polished sections.

For experiments performed at 7.5 and 10.0 GPa, the size of the jadeite crystals was too small for single crystal FTIR spectroscopy. Several attempts were made to synthesise larger crystals, but without success. Therefore, micropellets were made from the small jadeite crystals from both experiments by compressing the powder in a diamond-anvil cell. A small amount of each sample was loaded into a steel gasket, and the sample was compressed until it became optically transparent. Most of the load on the sample was then released to minimize residual stress in the sample. Pellets of 0.145 and 0.150-mm-thick were produced. Infrared spectra taken from these pellets inside the diamond anvil cell showed sharp absorption bands superimposed on a broad background most likely due to water on grain boundaries and in fluid inclusions. This broad background was removed by a spline fit.

Hydroxyl solubility in $NaAlSi_2O_6$ jadeite

Jadeite synthesis experiments

Experimental conditions for synthesis of jadeite and data on water solubility are listed in Table 1. Averaged compositions of jadeite crystals for each sample, determined by EMPA, are listed in Table 2. No evidence for the presence of Pt or Rh (above the detection limit of 0.02 wt %) was noted in the analyses. All of the samples are silica enriched to varying degrees. No trend of varying silica content with pressure is noted, and silica contents for the two samples synthesized at 2.0 GPa differ considerably. This may imply systematic overestimation of silica contents in some, if not all, of the samples (possibly as a result of the quartz standard used). Alternatively, some of the deviation in composition may actually be due to the presence of cation vacancies. Na totals are slightly lower than Al totals, possibly indicating the presence of M2 vacancies. Anomalously high silica contents in synthetic, Al-bearing enstatites were reported by Fockenberg and Schreyer (1997), and attributed to the presence of a Mg-Tschermak substitution mechanism (i.e. the presence of Mg vacancies). Similarly, the presence of silica exsolution lamellae in omphacites from ultra-high-pressure terrains has been attributed to the presence of a large Ca-Eskola component in pyroxenes at high pressure (as summarized by Dobrzhinetskaya et al. 2002). However, due to inaccuracies in measured oxide totals in Table 2 it is difficult to verify whether M2 vacancies are present solely based on EMPA results.

Table 1 Water solubility in $NaAlSi_2O_6$jadeite. Average water contents are derived from unpolarised FTIR spectra using the calibration of Paterson (1982)

Run No.	Method[1]	Pressure (GPa)	Time (hours)	Water content (wt. ppm H_2O)
HyJd4	1, PC	2.0	100	2722 or 451[2]
NeJd1	2, PC	2.0	261	470
HyJd5	1, PC	2.5	85	323
HyJd10	1, PC	3.0	172	305
HyJd13	1, PC	3.5	114	322
HyJd16	1, PC	4.0	121.5	88
NeJd3	2, MA	5.0	103	361
NeJd9	2, MA	7.5	72.5	132
NeJd7	2, MA	10.0	68.5	109

[1]Method 1 or 2 as explained in text, using piston-cylinder (PC) or multianvil (MA) apparatus

[2]Two values of water content are given corresponding to different interpretations of FTIR spectra (see text and Fig. 2 for more details)

Averaged unpolarized FTIR spectra for water-saturated jadeite are shown in Fig. 2. Polarized spectra obtained from one sample are shown in Fig. 3. The signal/noise ratio for polarized spectra is poorer than unpolarized spectra due to lower count rates and smaller areas from which spectra were obtained. All polarized and unpolarized spectra are characterized by a number of sharp peaks in the wavenumber range of 4000–2800 cm^{-1}, implying the presence of structurally-incorporated hydrogen. The characteristics of the absorption bands in jadeite spectra in polarized and unpolarized radiation, and the effects of pressure are listed in Table 3. Spectra obtained from the sample synthesised at 2.0 GPa using method 1 (HyJd4) contain a very broad feature centred on 3,430 cm^{-1}. This feature is not seen in spectra from samples synthesized at higher pressure. To test the reproducibility of this feature, another sample (NeJd1) was synthesized at 2.0 GPa using method 2. Spectra for this second sample do not contain the unusual feature, indicating that it represents some form of anomaly. However, spectra from sample HyJd4 were obtained from crack- and inclusion-free areas of large, euhedral crystals, so the reason for this anomaly is not immediately clear. Spectra obtained after careful polishing of the sample and after heating exclude the possibility that the anomaly is due to surface effects. Two water contents for the sample HyJd4 have, therefore, been calculated, one for the whole spectra, and one with the feature at 3430 cm^{-1} removed. The second value is in good agreement with, although slightly lower than, the value calculated for sample NeJd1. The slight difference in values is possibly due to the slight difference in run temperature. The calculated water content for sample HyJd16 is considerably lower than values for all other samples. No evidence for the presence of excess water was seen in this sample when the capsule was pierced and reweighed; this indicates that water was not held for the duration of the experiment.

A number of changes in FTIR spectra are noted as a function of increasing pressure (Table 3). Absorption

Table 2 Averaged compositions for jadeite samples, analysed by EMP. Compositions are given in weight percent oxides and in cations per formula unit based on 6 oxygens. Numbers in brackets are calculated values of 2σ for mean values

Exp. No.	Weight percent oxides				Cations per formula unit based on 6(0)			
	SiO_2	Na_2O	Al_2O_3	Total	Si	Na	Al	Total
HyJd4	60.97(54)	14.81(38)	24.39(62)	100.17(108)	2.12(2)	1.00(2)	1.00(2)	4.13(2)
NeJd1	60.68(5)	14.63(16)	25.07(7)	100.38(12)	2.02(1)	0.95(1)	0.99(1)	3.96(1)
HyJd5	59.35(31)	14.88(24)	24.81(32)	99.04(108)	2.10(1)	1.01(2)	1.03(1)	4.15(1)
HyJd10	60.53(50)	14.85(24)	24.90(31)	100.28(64)	2.11(9)	1.00(2)	1.02(1)	4.13(1)
HyJd13	60.27(65)	14.91(22)	24.74(22)	99.92(77)	2.11(1)	1.01(1)	1.02(1)	4.14(1)
HyJd16	60.99(36)	14.63(22)	25.18(23)	100.80(66)	2.03(1)	0.95(1)	0.98(1)	3.95(1)
NeJd3	59.93(46)	14.44(26)	24.95(72)	99.32(124)	2.02(1)	0.94(1)	0.99(2)	3.96(1)
NeJd9	60.70(52)	14.62(18)	24.90(26)	100.48(96)	2.03(1)	0.95(1)	0.98(1)	3.95(1)
NeJd7	60.61(83)	14.58(31)	24.87(34)	100.07(148)	2.03(1)	0.95(2)	0.98(1)	3.96(1)

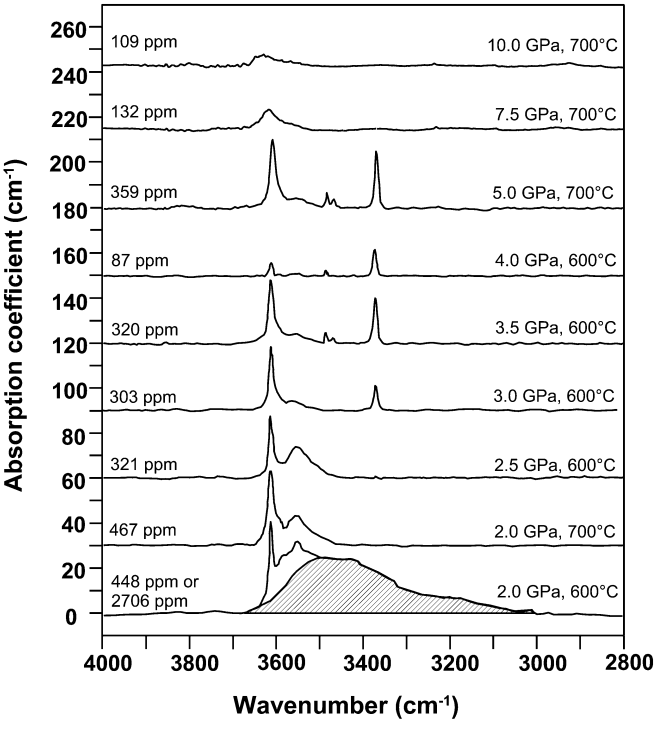

Fig. 2 Averaged, unpolarized FTIR spectra for synthetic, water-saturated jadeite synthesized between 2.0 and 10.0 GPa, 600–700 °C. Experimental conditions, and calculated water contents, in ppm H_2O, are given for each sample. Experiment at 4 GPa was not water-saturated

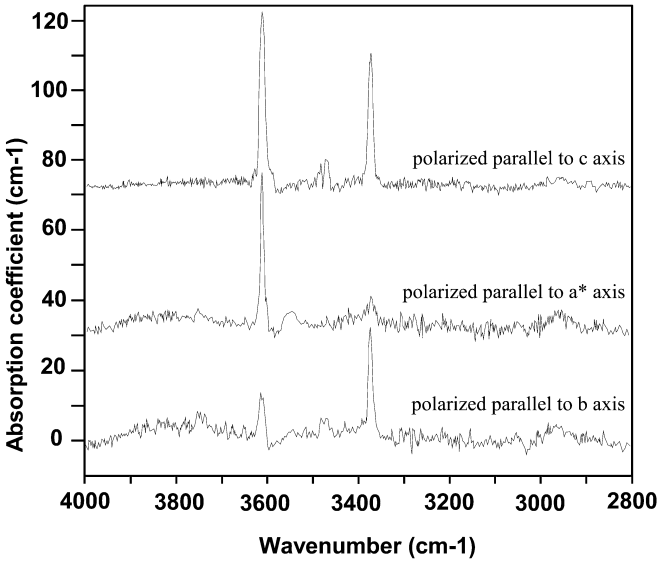

Fig. 3 Polarized spectra obtained from optically aligned jadeite crystal synthesized at 3.5 GPa, 600 °C

bands at 3488, 3469 and 3373 cm^{-1} all show an increase in peak height with increasing pressure from 3 to 5 GPa. In contrast, the absorption band at 3,550 cm^{-1} shows a marked decrease in peak height with increasing pressure, and is only prominent in spectra for samples synthesized below 3.0 GPa. Spectra from the two samples synthe-

Table 3 Characteristic of absorption bands from FTIR spectra for synthetic, water-saturated jadeite

Wavenumber (cm^{-1})	Characteristics	Band anisotropy in polarized spectra	Effect of increasing pressure
3613	Very sharp, prominent peak	Large component parallel to a* and c axes	Slight increase in peak height from 2.5 to 5 GPa, then decrease
3550	Broad hump	Largest component parallel to a* axis?	Marked decrease in peak height
3488	Small, sharp peak	Largest component parallel to c axis	Slight increase in peak height; only present in samples synthesised above 2.5 GPa, but absent above 5.0 GPa
3469	Very small peak	Largest component parallel to c axis	As above
3430	Very large, broad asymmetric feature. Possibly anomaly?	-	Only noted in HyJd4 sample
3373	Very sharp peak	Large component parallel to b and c axes	Large increase in peak height, but absent above 5.0 GPa

sized at 7.5 and 10.0 GPa, measured by the micropellet method, only contain the absorption band at 3613 cm^{-1}. This peak is shifted to slightly higher wavenumbers, and is slightly broadened in both spectra, possibly due to the effects of residual stress in the pellet. No other absorption bands in the high-pressure spectra are noted. In addition, the peak height for the absorption band at 3613 cm^{-1} decreases from 5.0 to 10.0 GPa. Fig. 4 shows a plot of calculated water content for pure jadeite synthesized from 2.0 to 10.0 GPa. Decreasing water contents could indicate that the partial molar volume of water in the fluid becomes smaller than the partial molar volume of water in jadeite at pressures greater than 5.0 GPa, leading to a decrease in solubility. Withers et al. (1998) noted a similar decrease in water solubility in pyrope above 6 GPa, consistent with the measured partial molar volume of water in hydrogarnet, which becomes greater than that in fluid at around this pressure. This has important implications for the capacity for jadeite, and possibly also for jadeite-rich omphacites, to act as significant repositories for water in subducting oceanic crust, and might imply that dehydration of omphacite eventually occurs during subduction.

The pressure dependence of water solubility in NAMs has been shown to be a function of water fugacity and the volume change of the host structure as a result of incorporation of hydrogen (Lu and Keppler 1997), and can be expressed in terms of a general solubility law,

$$c_{OH} = A\, f_{H_2O}^{n} \exp(-P\Delta V_S/RT) \quad (1)$$

where c_{OH} is water solubility (in ppm H_2O by weight), A is a temperature-dependent constant (ppm/bar^n), f_{H2O} is water fugacity (bars), P and T are run pressure (bars) and temperature (K), ΔV_s is the volume change of the host structure upon incorporation of OH (cm^3/mol), and R is the gas constant. Fig. 4 shows two fits of the general solubility law to the experimental data for water-saturated jadeite. Data were fitted for various values of n. A best fit is achieved for a value of $n = 0.5$, and values of 7.14 ppm/$bar^{0.5}$ and 8.019 cm^3/mol for A and ΔV_s, respectively, were refined. The refined value of ΔV_s is considerably smaller than the molar volume of liquid water, as would be expected, and is consistent with values published values for other NAMs (Bolfan-Casanova 2000). Values of ΔV_s derived for other values of n are unrealistically high. Water solubility in the synthetic jadeite is therefore proportional to the square root of water fugacity, implying that hydrogen is incorporated in the structure as isolated hydroxyl groups, and not as clusters of hydroxyl groups (3H replacing Al on the M1 site, or 4H replacing tetrahedral Si). Changes in IR spectra obtained from the synthetic jadeite as a function of pressure imply that there are several competing mechanisms for hydrogen incorporation in the structure. The fitted solubility law therefore only describes the overall trend in solubility with increasing pressure, and a perfect fit of the solubility law to the experimental data for jadeite is not expected.

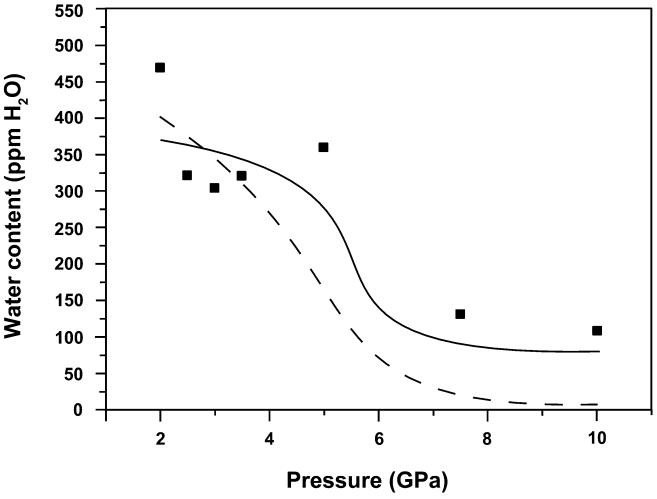

Fig. 4 Water solubility in synthetic jadeite as a function of pressure, fitted to the general solubility law, $c_{OH} = A\, f_{H2O}^{n} \exp(-P\Delta V_{Solid}/RT)$, for values of $n = 0.5$ (*solid line*) and $n = 1$ (*dashed line*). See text for more details on data fitting

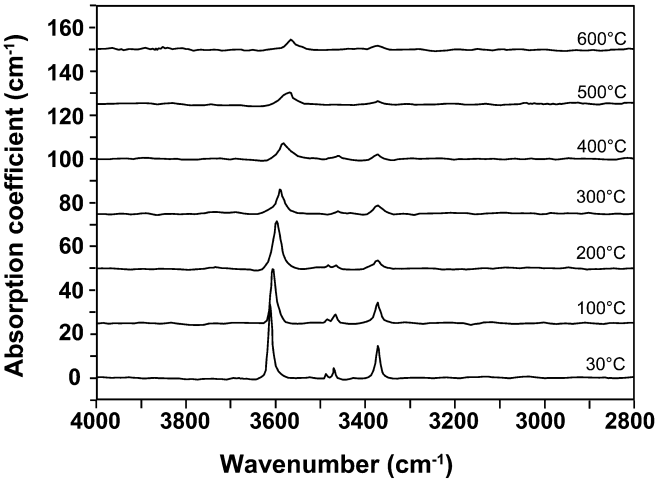

Fig. 5 High-temperature FTIR spectra for synthetic jadeite (synthesized at 3.0 GPa, 600 °C)

High-temperature spectroscopy

Using a heating stage, FTIR spectra were obtained, with increasing temperature, from one crystal from sample HyJd10 (synthesized at 3 GPa). High temperature spectra from this sample are shown in Fig. 5. The absorption bands at 3613, 3488 and 3,470 cm^{-1} all exhibit a decrease in frequency with increasing temperature. The absorption band at 3,373 cm^{-1} shows no shift in frequency over the temperature range studied. With increasing temperature, all bands broaden significantly. Lu and Keppler (1997) noted the similar behaviour upon heating for absorption bands in natural pyrope, and attributed this behaviour to weak or negligible hydrogen bonding in OH groups (a frequency increase would be expected for OH groups experiencing strong hydrogen

Table 4 Possible hydrogen incorporation mechanisms in water-saturated jadeite

Mechanism No.	Description of incorporation mechanism	Bond length (O...O) Å	Angle of vector relative to axes[1]			Possible assignment (wavenumber cm^{-1})
			X	Y	Z	
1	Between O2 and O1 along shared edge of M1 and M2 polyhedra	2.818	33.94	60.77	51.69	3550
2	Between O2 and O3 along edge of M2 polyhedron	3.451	36.14	50.57	72.27	3550
3	Between 2 O1 along edge of M1 octahedron (two different directions)	2.918	90.00	63.39	26.56	3488 and 3469
4	Between 2 O3 along edge of M2 polyhedron	2.973	6.81	87.69	88.82	3550
5	Between 2 O3 along edge of M2 polyhedron	3.266	25.33	90.00	38.70	3613
6	Between O1 and O2 along edge of M1 octahedron	2.678	83.91	59.08	34.95	3373

[1]Angles are given relative to principle crystallographic axes (i.e. not orthogonal)

bonding due to thermal expansion of interatomic distances leading to decreasing bond strength). Shifts in absorption band frequency are probably controlled by thermal expansivity of the sites of hydrogen incorporation. Differences between frequency shifts for the absorption bands at 3,613, 3,488 and 3,469, and 3,373 cm^{-1} therefore indicates different modes of hydrogen incorporation. Absorption band broadening with increasing temperature may represent interaction with lattice vibrations (Lu and Keppler 1997); above 600 °C, extensive broadening and reduction in resolution meant that it was no longer possible to distinguish absorption bands in the spectra. Spectra for the sample obtained before and after heating are essentially identical, except for a slight reduction in peak height for all of the absorption bands, possibly indicating the onset of hydrogen diffusion during heating. The sample was heated to 700 °C over approximately 30 min.

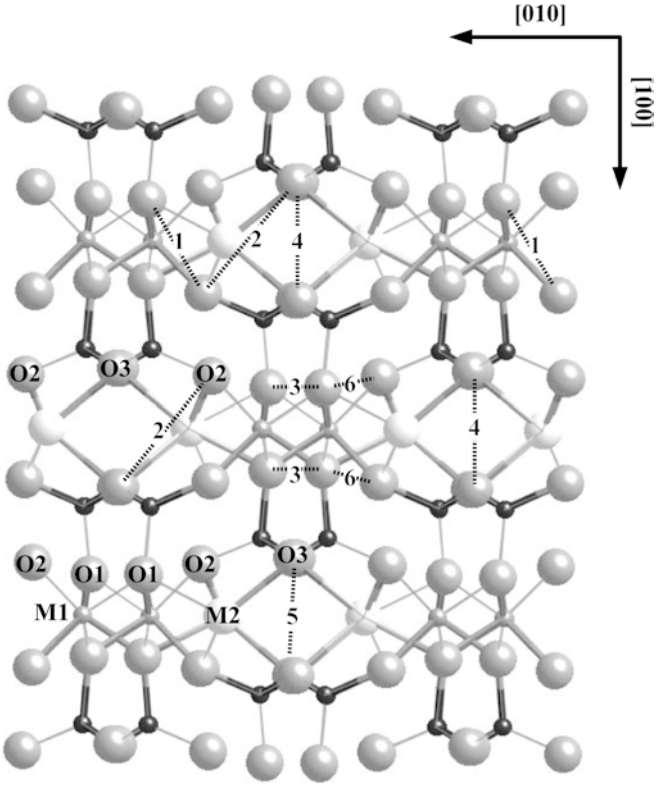

Fig. 6 Jadeite model cut perpendicular to (001) showing proposed hydrogen incorporation mechanisms in synthetic, water-saturated jadeite. Al (M1) sites are shown as *small grey spheres*, Na (M2) sites as *large white spheres*, Si sites as *small black spheres* and O sites as *large grey spheres*. Selected oxygen sites are labelled. Hydrogen incorporation mechanisms are shown as *dotted lines* between oxygen atoms, and imply hydrogen associated with one oxygen, and vibration of the OH dipole in the direction of the adjacent oxygen. For mechanism 5, the lower O3 atom is not visible in the plot

Assignment of absorption bands in IR spectra for jadeite

Nakamoto et al. (1955) and Libowitzky (1999) demonstrated the correlation between O-O distances in a number hydrous and nominally anhydrous minerals with O-H stretching frequencies from IR spectra. This correlation presupposes that the direction of vibration of OH dipoles is approximately collinear with O-O directions in the host phase, an assumption which holds true for most phases investigated. Using the correlation of Libowitzky (1999), in combination with data on absorption band anisotropy, an initial assignment of the absorption bands in IR spectra for synthetic, water-saturated jadeite has been attempted. O-O distances were taken from Prewitt and Burnham (1966). Proposed incorporation mechanisms consistent with data for jadeite are listed in Table 4, and shown schematically in Fig. 6. Using the method outlined, up to 20 possible modes of hydrogen incorporation in jadeite were identified. Previous investigations of the incorporation of trace amounts of hydrogen in nominally anhydrous phases have shown that hydrogen is either incorporated along the edges or faces of cation polyhedra or OH bonds vibrate in the direction of cation vacancies (e.g. Beran and Zemann 1986; Smyth et al. 1991; Stalder and Skogby 2002; Swope et al. 1995). Therefore, for assigning absorption bands in jadeite spectra, mechanisms where hydrogen would be incorporated along the edges or faces of cation polyhedra or across vacant polyhedral sites were preferred. Six possible mechanisms are listed in Table 4. O-O distances around tetrahedral

Table 5 Experimental conditions and water solubility in synthetic, jadeite-rich pyroxenes. Average water contents derived from unpolarized FTIR spectra using the calibration of Paterson (1982)

Run No.	Bulk Composition	Pressure (GPa)	Time (hours)	Water content (wt. ppm H_2O)
Jdomp1	$Jd_{0.76}Di_{0.24}$	2.5	116	458
JdCaEs1	$Jd_{0.9}CaEs_{0.1}$	2.0	125	780

sites in jadeite are too short to explain any of the absorption bands seen in IR spectra. Instead, the most favourable mechanisms identified using this technique involve hydrogen incorporation along the edges of M1 and M2 polyhedra. Vacancies on M2 sites are more favourable in pure end-member jadeite because of the lower charge of the Na^+ cation, and are also suggested by the EMPA results. Mechanisms 1, 2, 4 and 5 all involve hydrogen incorporation along edges of M2 polyhedra (as shown in Fig. 6). Mechanism 5 is the only proposed mechanism which can explain the position and nature of the absorption band at 3,613 cm^{-1}. Mechanisms 1, 2 and 4 are all possible candidates to explain the absorption band at 3,550 cm^{-1}. Of these, mechanisms 1 and 2 would appear more favourable, because they would imply hydrogen association with the highly underbonded O2 site. Mechanism 2 is comparable to a mechanism for hydrogen incorporation in diopside proposed by Beran (1976), where hydrogen is associated with the underbonded O2 site, and vibrates in the direction of the O3 site. Mechanisms 1, 2, 4 and 5 would be favourable if M2 vacancies existed in the jadeite structure, with hydrogen incorporation charge-balancing the absence of Na^+. In contrast, mechanisms 3 and 6 imply incorporation of hydrogen along edges of M1 octahedra. Mechanism 6 is the only mechanism found which appears to explain the absorption band at 3,373 cm^{-1}. Mechanism 3 actually describes two distinct modes of hydrogen incorporation, and could therefore be used to account for the two small absorption bands seen at 3,488 and 3,469 cm^{-1}. Hydrogen incorporation in jadeite charge-balanced by vacancies on the M1 site appears much less likely because M1 sites are occupied with Al^{3+}. Hydrogen incorporation by mechanisms 3 and 6 in combination would only partially, but not completely, compensate for the charge-imbalance resulting from M1 vacancies. In addition, the effect of pressure on water solubility in jadeite suggests that hydrogen is incorporated as isolated hydroxyl groups, and not as clusters. In this study, all the jadeite synthesis experiments were nominally performed in the Na_2O–Al_2O_3–SiO_2–H_2O system. However, it is possible that ppm levels of additional oxides are present in the starting mix, and therefore substitution of lower valency cations (e.g. Fe, a trace element contaminant in the $Al(OH)_3$ used in the starting mix) onto the M1 site in combination with hydrogen incorporation could be envisaged. The model of hydrogen incorporation in jadeite proposed here is consistent with the results of the fit of the solubility law to the experimental data; i.e. hydrogen is incorporated in the jadeite structure via a number of independently operating mechanisms, and not by the formation of complicated defect clusters involving several hydroxyl groups. In contrast, Rauch and Keppler (2002) found that water was incorporated in pure, water-saturated enstatite as hydroxyl pairs, possibly as a direct substitution for Mg^{2+} cations.

In an investigation of water solubility in natural omphacites, Smyth et al. (1991) noted a positive correlation between water solubility and the number of M2 vacancies in jadeite-rich samples. Based on this correlation, Smyth et al. (1991) suggested that the dominant mode of hydrogen incorporation involved hydrogen associated with the highly underbonded O_2 site, with OH bonds vibrating in the direction of M2 vacancies. However, for end-member jadeite, O-O distances across the M2 site are too long for this mechanism to explain any of the absorption bands seen in the IR spectra.

Hydroxyl solubility in Na-rich pyroxenes

Additional synthesis experiments were conducted to determine the effect of small additional components on the solubility and speciation of hydrogen in jadeite. Two bulk compositions were prepared, one for a jadeite-rich composition with a small Ca-Eskola ($Ca_{0.5}\square_{0.5}AlSi_2O_6$) component, and one for a jadeite-rich composition with a diopside ($CaMgSi_2O_6$) component. For the jadeite-diopside starting mix, a bulk composition corresponding to $Jd_{0.76}Di_{0.24}$ was prepared, comparable to the jadeite:diopside ratio in the pyroxene SBB-1 described by Smyth et al (1991) which contained 1,840 ppm H_2O. For the jadeite-Ca-Eskola starting mix, a bulk composition corresponding to $Jd_{0.9}Ca$-$Es_{0.1}$ was chosen. Experiments were conducted using the piston-cylinder apparatus and method 1, as described above.

Experimental conditions and calculated water contents are listed in Table 5. Averaged FTIR spectra for both samples are shown in Fig. 7, and averaged compositions are listed in Table 6. Crystal sizes in both experiments were noticeably smaller than in pure jadeite experiments, and as a result, resolution of FTIR spectra is poorer. EMPA revealed variation in crystal composition in both samples, although there was no evidence for compositional zoning within crystals. Variation in composition implies lack of chemical equilibrium, probably resulting from the temperature-fluxing method used to grow large crystals, and from the low temperature of sample synthesis. For sample Jdomp1, the

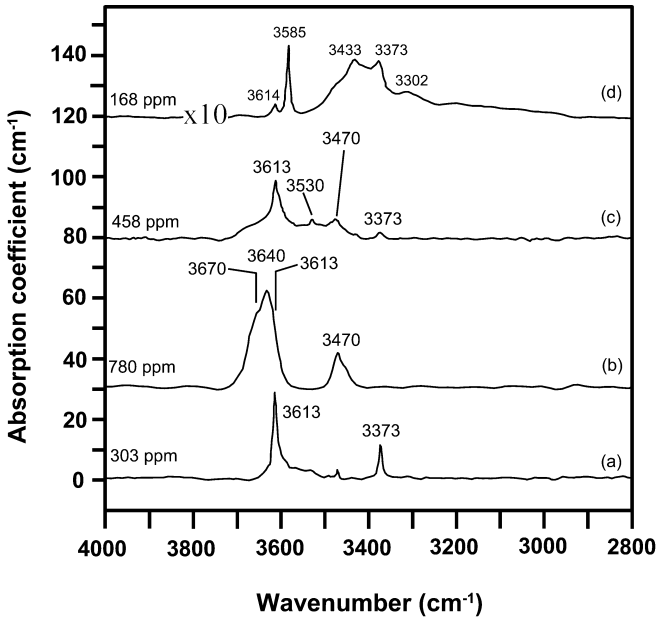

Fig. 7 Averaged FTIR spectra for samples synthesized along the jadeite-diopside tie-line. **a** HyJd10, pure jadeite synthesized at 3.0 GPa, 600 °C (b) JdCaEs1, $Jd_{0.9}CaEs_{0.1}$ synthesized at 2.0 GPa, 600 °C **c** Jdomp1, $Jd_{0.4}Di_{0.5}CaTs_{0.1}$, synthesized at 2.5 GPa, 600 °C **d** pure diopside, synthesized at 1.5 GPa 1100 °C (Rauch 2000), multiplied by 10 for clarity. Calculated water contents, expressed at ppm H_2O, for each sample are given

average composition can be expressed in terms of jadeite, diopside and Ca-Tschermak ($CaAl_2SiO_6$) components: $Jd_{0.4}Di_{0.5}CaTs_{0.1}$. The presence of a small Ca-Tschermak component implies mixing of Al and Si on the tetrahedral site. The jadeite:diopside ratio of the sample differs considerably from the ratio of the starting mix. The averaged FTIR spectra for Jdomp1 show many features similar to spectra for pure jadeite, with peaks at 3,613, 3,470 and 3,373 cm^{-1}. There is also at least one additional peak at 3,530 cm^{-1}. All peaks are noticeably broader in spectra for Jdomp1 than in spectra for pure jadeite, and the peaks at 3,470 and 3,373 cm^{-1} are slightly larger than the peaks in jadeite synthesised under the same conditions. The average calculated water content for sample Jdomp1 is noticeably higher than the corresponding value for pure jadeite. No difference between spectra for different crystals as a function of varying composition was noted. Similarity between FTIR spectra for synthetic jadeite and synthetic omphacite suggests that mechanisms for hydrogen incorporation in both are probably similar. In addition, these results suggest that the presence of Al on tetrahedral sites in omphacite has only a limited effect on hydrogen incorporation in omphacite. This is consistent with all mechanisms of hydrogen incorporation described in Table 4, and the mechanism outlined by Smyth et al. (1991) where hydrogen incorporation is associated with vacancies on the M2 and occupancy of M1 sites. Furthermore, these results suggest that hydrogen incorporation in pure jadeite may be used as a model for hydrogen incorporation in more complex jadeite-diopside solid solutions. In contrast, FTIR spectra for synthetic pure diopside (Fig. 7) differ considerably from the synthetic omphacite spectra.

The composition of sample JdCaEs1 can be expressed as $Jd_{0.9}CaEs_{0.1}$ and is close to the that of the bulk composition, although some variation in composition between crystals is noted. High values for the number of Si^{4+} cations pfu excludes the presence of a small Ca-Tschermak component. The FTIR spectra for JdCaEs1 samples are characterised by two large features, a large peak centred around 3,640 cm^{-1}, possibly with a shoulder at around 3,670 cm^{-1}, and a smaller, slightly asymmetric peak at 3,470 cm^{-1}. The peak at 3,640 cm^{-1} could conceivably be analogous to the 3,613 cm^{-1} peak in pure jadeite, shifted to higher wavenumbers as a result of NNN forces. This would be consistent with the assignation of the band at 3,613 cm^{-1} proposed in Table 4 (i.e. mechanism 5), whereby hydrogen sits along an edge of the M2 polyhedron. Increase in peak height for absorption bands in spectra obtained for sample JdCaEs1 could, therefore, be due to the increase in the number of M2 vacancies. The absorption band at 3,470 cm^{-1} in spectra from JdCaEs1 is also considerably larger than in jadeite spectra, or in spectra for sample Jdomp1. This supports the assignation of the band at 3,470 cm^{-1} by Smyth et al. (1991), with hydrogen

Table 6 Averaged compositions for Na-rich omphacite samples, analysed by EMP. Compositions are given in weight percent oxides, cations per formula unit based on 6 oxygens, and the proportion of each end member. Values of 2 sigma, representing variation in data from mean values, are given as values on the last digit

Experiment						
	Weight percent oxides					
	SiO_2	CaO	Na_2O	Al_2O_3	MgO	Total
Jdomp1	54.87(40)	15.87(80)	5.21(54)	14.35(80)	10.81(70)	101.16(70)
JdCaEs1	59.85(63)	0.99(24)	13.87(21)	24.66(47)	–	99.51(113)
	Cations p.f.u. based on 6(O)					
	Si	Ca	Na	Al	Mg	Total
Jdomp1	1.90(1)	0.59(3)	0.35(4)	0.59(3)	0.56(4)	3.98(1)
JdCaEs1	2.02(1)	0.04(1)	0.91(2)	0.98(1)	–	3.95(1)
	Proportion end-members					
	Jadeite	Ca-Eskola	Diopside	Ca-Tschermak	Total	
Jdomp1	0.37(4)	–	0.53(3)	0.10(2)	0.99(1)	
JdCaEs1	0.91(2)	0.07(2)	–	–	0.98(1)	

associated with the O2 site. Calculated water contents for the sample are the highest of all the samples studied in this investigation. This is consistent with investigations of water contents in natural omphacites (Katayama and Nakashima 2003; Smyth et al. 1991), where a correlation between water contents and Ca-Eskola content is noted.

Comparison of IR spectra for natural and synthetic samples

Figure 8 shows FTIR spectra for several *C*2/*c* omphacites from high-pressure eclogitic terrains. Spectra (a) and (b) are from the study of Smyth et al. (1991) and were obtained from diopside and jadeite-rich samples respectively. Spectra (b) exhibits one large peak at 3,470 cm^{-1}. In contrast, spectra for synthetic jadeite and omphacite from the present study are characterized by a number of distinct absorption bands. However, spectra for all synthetic samples (except lower pressure jadeite samples) have a small absorption band at 3,470 cm^{-1}. In the spectra for sample JdCaEs1, the peak height of this band is increased relative to spectra for pure jadeite. The Ca-Eskola component of sample JdCaEs1 is close to that of the pyroxene from which spectra (b) was obtained.

Jadeite and omphacite spectra from the present study appear to resemble more closely spectra from ultrahigh-pressure omphacites obtained by Katayama and Nakashima (2003) (Fig. 8c). They identified three groups of absorption bands at 3,600–3,625, 3,500–3,530 and 3,440–3,460 cm^{-1}, which appear comparable to the absorption bands at 3,613 and 3,470 in jadeite and Jdomp1 spectra and the band at 3,530 only noted in Jdomp1 spectra. Katayama and Nakashima (2003) also noted changes in relative peak heights between the three groups of absorption bands as a function of pressure. This is in accordance with the present results on hydrogen incorporation in pure jadeite, and strongly indicates that hydrogen is incorporated in the jadeite and omphacite structures as independent hydroxyl groups, and not as clusters of hydroxyl groups. Absorption bands in spectra from natural samples, and from synthetic solid solutions, are much broader than in spectra obtained from the pure jadeite. This implies an increase in disorder of the hydrogen positions, which would be expected due to mixed occupancy of the cation sites. Spectra from synthetic samples contain more fine detail than published spectra from natural omphacites. The effect of peak broadening in natural samples may be to mask some of the fine detail of absorption bands in IR spectra.

Water contents in natural samples are higher than those determined for the synthetic samples in this study. Again, this may be due to the presence of additional components in natural samples. Most noticeably, both samples studied by Smyth et al. (1991) contained a significant hedenbergite component.

Conclusions

Results from the present investigation suggest that there are at least 5 modes of hydrogen incorporation in synthetic, water-saturated jadeite. Additional experiments using jadeite + diopside and jadeite + Ca-Eskola starting mixtures suggest that jadeite provides a good model for considering hydrogen incorporation in more complex omphacite compositions. This is also supported by comparison between the IR spectra for jadeite and omphacite in this study with recently published IR spectra obtained from natural omphacites from an UHP terrain by Katayama and Nakashima (2003). Spectra

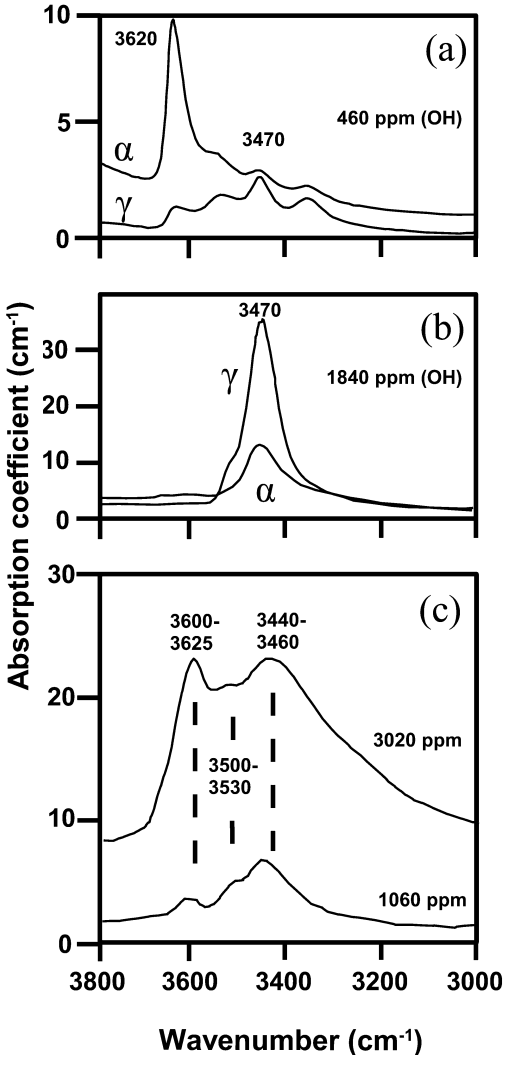

Fig. 8 FTIR spectra for natural omphacites from high-pressure terrains **a** Smyth et al. (1991), two polarized spectra from diopside-rich sample ($Di_{85}Hd_6Ac_5CaTs_3$). **b** Smyth et al. (1991), two polarized spectra from jadeite-rich omphacite ($Jd_{59}Di_{20}Hd_8CaEs_{12}$). **c** Katayama and Nakashima (2003), two unpolarised spectra obtained from omphacites (composition approximately 1:1 Jd:Di) from diamond-grade (*upper*) and quartz-bearing (*lower*) eclogites. Numbers refer to wave numbers (cm^{-1}) of absorption bands

obtained from natural, jadeite-rich omphacite by Smyth et al. (1991) are dominated by one large absorption band at 3,470 cm^{-1}, which they suggested was related to the presence of M2 vacancies. Results from this study and the study by Katayama and Nakashima (2003) indicate that a number of additional hydrogen incorporation mechanisms may also be present in jadeite and omphacite. Using the correlation of Libowitzky (1999), we suggest that hydrogen incorporation in jadeite and omphacite could also be related to the presence of lower valency cations on the M1 site. Results do, however, suggest that hydrogen incorporation related to occupancy of the tetrahedral site in both structures is unlikely. The effect of pressure (i.e. f_{H2O}) on water solubility in jadeite implies that hydrogen is incorporated as isolated hydroxyl groups, and not as clusters. The addition of a small Ca-Eskola component to jadeite increases the amount of water incorporated by the structure considerably. This verifies the importance of considering the number of M2 vacancies in controlling the solubility of hydrogen in omphacite.

Absorption bands in IR spectra for pure jadeite are characteristically sharp (except for the slightly broader band at 3,550 cm^{-1}). One effect of adding additional components to the system appears to be significant broadening of all absorption bands. This is consistent with published IR spectra for natural omphacites, which are characterized by several broad features over the wavenumber range corresponding to OH stretching frequencies. It is possible that such broad features mask some of the finer detail in IR spectra.

A number of changes in IR spectra for jadeite are noted as a function of increasing pressure, indicating changes in mechanisms for hydrogen incorporation. Most importantly, at pressures above 5 GPa, only the absorption band at 3,613 cm^{-1} is seen in IR spectra, and from 5 to 10 GPa, there is a decrease in hydrogen solubility. No experimental information is available on hydrogen solubility in omphacite as a function of pressure, or whether the trend of decreasing hydrogen solubility in jadeite above 5 GPa is applicable to more complex solid solutions. Decreasing hydrogen solubility in omphacite with increasing pressure would have an important influence on the capacity of subducting oceanic crust to retain water, and have major implications for consideration of the internal water cycle of the earth. However, solid solution of jadeite with diopside and in particular, with Ca-Eskola component leads to a drastic increase of water solubility. It is therefore conceivable that bulk composition has a more important effect on the capacity of omphacite to store water than pressure and temperature. In any case will omphacite be the major carrier of water in a subducted eclogite after the breakdown of hydrous minerals.

Acknowledgements The authors would like to thank Dan Frost for help with multi-anvil experiments, Hubert Schulze for sample preparation, Georg Herrmansdörfer and Heinz Fischer for manufacturing components for piston-cylinder and multi-anvil apparatus and Detlef Kaube for assistance with EMPA. This manuscript benefited greatly from detailed reviews by R. Oberti and R. Stalder. This work was supported by the EU Hydrospec network (Improving Human Potential Programme).

References

Bell D, Rossman G (1992) Water in Earth's mantle: the role of nominally anhydrous minerals. Science 255:1391–1397

Beran A (1976) Messung des Ultrarot-Pleochroismus von Mineralen. XIV. Der Pleochroismus der OH-Streckfrequenz in Diopsid. Tscherm Min Petrol Mitt 23:79–85

Beran A, Zemann J (1986) The pleochroism of a gem-quality enstatite in the region of the OH stretching frequency, with a stereochemical interpretation. Tscherm Min Petrol Mitt 35:19–25

Bolfan-Cassanova N (2000) The distribution of water in the Earth's mantle: an experimental and infrared spectroscopic study. PhD thesis, Universitaet Bayreuth, Bayreuth

Bromiley GD, Pawley A (2002) The high-pressure stability of Mg-sursassite in a model hydrous peridotite: a possible mechanism for the deep subduction of significant volumes of H_2O. Contrib Mineral Petrol 142:714–723

Cameron M, Papike J (1981) Structural and chemical variations in pyroxenes. Am Mineral 66:1–50

Dobrzhinetskaya L, Schweinehage R, Massonne H-J, Green H (2002) Silica precipitates in omphacite from eclogite at Alpe Arami, Switzerland: evidence of deep subduction. J Metamorph Geol 20:481

Fockenberg T, Schreyer W (1997) Synthesis and chemistry of unusual excess-Si aluminous enstatite in the system MgO–Al_2O_3–SiO_2 (MAS). Eur J Mineral 9:509–518

Gasparik T (1986) Experimental study of subsolidus phase relations and mixing properties of clinopyroxene in the silica-saturated system CaO–MgO–Al_2O_3–SiO_2. Am Mineral 71:686–693

Green H, Dobrzhinetskaya L, Bozhilov K (2000) Mineralogical and experimental evidence for very deep exhumation from subduction zones. J Geodynam 30(1–2):61–76

Hawthorne F, Welch M, Della Ventura G, Liu S, Robert J, Jenkins D (2000) Short-range order in synthetic aluminous tremolites: an infrared and triple-quantum MAS NMR study. Am Mineral 85:1716–1724

Holland T (1990) The reaction albite = jadeite + quartz determined in the range 600–1200 °C. Am Mineral 65:129–134

Ingrin J, Skogby H (2000) Hydrogen in nominally anhydrous upper-mantle minerals: concentration levels and implications. Eur J Mineral 12:543–570

Katayama I, Nakashima S (2003) Hydroxyl in clinopyroxene from the deep subducted crust: evidence for H_2O transport into the mantle. Am Mineral 88:229–234

Libowitzky E (1999) Correlation of O-H stretching frequencies and O-H···O hydrogen bond lengths in minerals. Monatsh Chemie 130(8):1047–1059

Libowitzky E, Rossman G (1997) An IR absorption calibration for water in minerals. Am Mineral 82:1111–1115

Lu R, Keppler H (1997) Water solubility in pyrope to 100 kbar. Contrib Mineral Petrol 129:35–42

Malinovskaya E, Doroshev A, Bulatov V, Brey G (1991) Clinopyroxenes of $CaMgSi_2O_6$–$CaAl_2SiO_6$–$Ca_{0.5}AlSi_2O_6$ series in association with anorthite, quartz, coesite and garnet. Geokhimiya 2:216–226

Nakamoto K, Margoshes M, Rundle RE (1955) Stretching frequencies as a function of distances in hydrogen bonds. J Am Chem Soc 77:6480–6488

Paterson M (1982) The determination of hydroxyl by infrared absorption in quartz, silicate glasses and similar materials. Bull Mineral 105:20–29

Prewitt CT, Burnham CW (1966) The crystal structure of jadeite, $NaAlSi_2O_6$. Am Mineral 7:956–976

Rauch, M (2000) Der Einbau von Wasser in Pyroxene. Ph D thesis, Universitaet Bayreuth, Bayreuth

Rauch M, Keppler H (2002) Water solubility in orthopyroxene. Contrib Mineral Petrol 143:525–536
Rossi G, Smith D, Ungaretti L, Domeneghetti M (1983) Crystal-chemistry and cation ordering in the system diopside-jadeite: a detailed study by crystal structure refinement. Contrib Mineral Petrol 83:247–258
Schmädicke E, Müller W (2000) Unusual exsolution phenomena in omphacite and partial replacement of phengite by phlogopite + kyanite in an eclogite from the Erzgebirge. Contrib Mineral Petrol 139:629–642
Schmidt M (1993) Phase-relations and compositions in tonalite as a function of pressure -an experimental study at 650 °C. Am J Sci 10:1011–1060
Schmidt M, Poli S (1998) Experimentally based water budgets for dehydrating slabs and consequences for arc magma generation. Earth Planet Sci Lett 163:361–379
Skogby H (1994) OH incorporation in synthetic clinopyroxene. Am Mineral 79:240–249
Skogby H, Bell D, Rossman G (1990) Hydroxide in pyroxene: variations in the natural environment. Am Mineral 75:764–774
Smyth J, Bell D, Rossman G (1991) Incorporation of hydroxyl in upper-mantle clinopyroxenes. Nature 351:732–735
Stalder R, Skogby H (2002) Hydrogen incorporation in enstatite. Eur J Mineral 14:1139–1144
Swope R, Smyth J, Larson A (1995) H in rutile compounds: I. single-crystal neutron and X-ray diffraction study of H in rutile. Am Mineral 80:448–453
Terry M, Bromiley GD, Robinson P (2003) Determination of equilibrium water content and compositon of omphacitic pyroxene in a UHP kyanite-eclogite, Western Norway. Geophys Res Abs 5:08698.
Walker D (1991) Lubrication, gasketing, and precision in multi-anvil experiments. Am Mineral 76:1092–1100
Walker D, Carpenter M, Hitch C (1990) Some simplifications to multianvil devices for high-pressure experiments. Am Mineral 75:1020–1028
Withers A, Wood B, Carroll M (1998) The OH content of pyrope at high pressure. Chem Geol 147:161–171
Zhang R, Liou J (1999) Exsolution lamellae in minerals from ultrahigh-pressure rocks. Int Geol Rev 41(11):981–993
Zhang R, Liou J, Ernst W, Coleman R, Sobolev N, Shatsky V (1997) Metamorphic evolution of diamond-bearing and associated rocks from the Kokchetav Massif, northern Kazakhstan. JMetamorphGeol 15:479–496